We are IntechOpen, the world's leading publisher of Open Access books Built by scientists, for scientists

6,900
Open access books available

185,000
International authors and editors

200M
Downloads

Our authors are among the

154
Countries delivered to

TOP 1%
most cited scientists

12.2%
Contributors from top 500 universities



WEB OF SCIENCE™

Selection of our books indexed in the Book Citation Index in Web of Science™ Core Collection (BKCI)

Interested in publishing with us?
Contact book.department@intechopen.com

Numbers displayed above are based on latest data collected.
For more information visit www.intechopen.com



Chapter

Perovskite-Type Lanthanum Cobaltite $LaCoO_3$: Aspects of Processing Route toward Practical Applications

Mirela Dragan, Stanica Enache, Mihai Varlam and Konstantin Petrov

Abstract

Lanthanum cobaltite ($LaCoO_3$) perovskite-type oxide is an important conductive ceramic material finding a broad range of technical applications. Physical and chemical properties of the final lanthanum cobalt oxide powder material obtained are strongly dependent on the method of preparation. Taking in account these considerations, we focus our investigation on the solid state reaction process. The characterization of prepared lanthanum cobalt oxide material was studied by using X-ray diffractometry (XRD), scanning electron microscopy (SEM), thermogravimetry-differential scanning calorimetry (TG-DSC), and conduction properties. Following the experimental results, it can be concluded that with proper improvement, the solid state reaction process may also provide an efficient preparation method for perovskite-type $LaCoO_3$ powder. Important to mention is that we looked into the aspects to produce again same which showed consistently reproducibility of batch to batch powder properties. This is a key factor to overcome a successful commercialization of new material synthesis development.

Keywords: perovskite, $LaCoO_3$, oxide powders synthesis, solid state reaction

1. Introduction

The continuous interaction between structure and properties allows several intrinsic properties of perovskite materials to advance a very broad range of practical applications. These oxides are being increasingly applied to electronic and magnetic materials [1–3], automotive exhaust and water splitting catalysts [4, 5], and electrode materials for fuel cells and batteries [6, 7]. Among these perovskites, the cobalt-based type $LaCoO_3$ perovskite ignited interest in the research since the early 1960s [8, 9] and continues to be the material of the moment. $LaCoO_3$ perovskite has been shown to have promising catalytic activity for oxygen evolution reaction (OER) [10, 11]. Lanthanum, La, is a relatively large cation and gives structural stability to the catalyst. Rare-earth oxides with full or partially filled inner shells of lanthanide ions would involve the 4f electrons. The 4f electrons contribute to the density of states around the Fermi level, and degenerate strongly, the bandwidth is

narrow and steep. The presence of La^{3+} with no 4f electrons is beneficial because the electrical conductivity increases and the effective mass decreases [12].

Cobalt, Co, cation, a transition metal with smaller size than La cation, is responsible for catalytic activity. In its compounds, cobalt nearly always exhibits a +2 or +3 oxidation state, although states +4, +1, 0, and −1 are also known [13]. The outer electrons of the element are either in the 3d or 4s subshell. Cobalt chemistry is dominated by the behavior of the 3d electrons. Oxidation state of Co helps the $LaCoO_3$ catalytic activity for OER which can be associated with Co^{3+} oxidation state. Co^{3+} active sites by absorption of HO^- may act as reactants for OER [14]. Electrocatalysis at room temperature, in correlation to the fundamental electronic structure, is still not fully clarified. For Co_3O_4 with the band gap of 1.9 eV and $LaCoO_3$ with about 0.8 eV, the resistivity is 10^4 and 10 Ωcm, respectively [15, 16].

On the other hand, crystallographic structure is important for the functional properties of the oxides. For perovskite, the ideal cubic structure goes through different structural distortions due to the ionic radii differences.

The equation determined by Goldschmidt correlates crystal structures geometrically in terms of the ionic packing using the Goldschmidt's tolerance factor t. For a stable perovskite structure, the tolerance factor should have values between 0.75 and 1; otherwise, the ideal cubic structure is a distorted structure. Mathematical expression involving the unit cell length ratio, here r_{La}, r_{Co}, and r_O, is the ionic radii for La, Co, and O respectively; t is given as:

$$t = \frac{(r_{La} + r_O)}{\sqrt{2}\,(r_{Co} + r_O)} \tag{1}$$

Taking in consideration the Shannon crystal ionic radii for all ions along with their coordination numbers [17], the calculated tolerance factor of $LaCoO_3$ is 0.97 for Co^{3+} and 0.905 for Co^{2+}.

Experimentally, by neutron diffraction technique, the change of lattice parameter with temperature has been observed when the lattice length and angle become longer and smaller, respectively, when temperature increases [18].

The crystal structure of $LaCoO_3$, as shown in **Figure 1**—La atoms, in blue, at corners; O atoms, in red, on face centers; and Co atoms, in green, at the center of the lattice—is a rhombohedron having R3c symmetry at room temperature. This is considered as the most stable: $LaCoO_3$ structure up to around 1698 K when the crystal is cubic [19].

Not only the temperature but also the oxygen partial pressure of environments, $p(O_2)$ leads the $LaCoO_3$ to a wide range of oxygen deficiency represented by the formula $LaCoO_{3-\delta}$ with δ being the oxygen deficiency. It is observed that moderate oxygen deficiency in $LaCoO_{3-\delta}$ causes a slight distortion of the ideal cubic structure which is rombohedral [20].

Since the structure-properties relations are strongly dependent on the preparation method, a lot of interest is focused on their synthesis which ultimately determines its potential applications.

The aim of this research is to explore the possibility to improve the solid state preparation method for obtaining $LaCoO_3$ micro- and nanocrystals, which may contribute to the development of a large-scale production route of $LaCoO_3$ with controlled properties.

Numerous routes to prepare perovskite powders have been proposed. These address various problems involved in the preparation of polycrystalline perovskite powder with single phase, resulting in various microstructures and properties.

Among the adopted techniques, solid state reaction [21], mechanochemical processing [22], Pechini method [23], combustion synthesis [24], sol-gel method [25], and microwave route [26] are widely used.

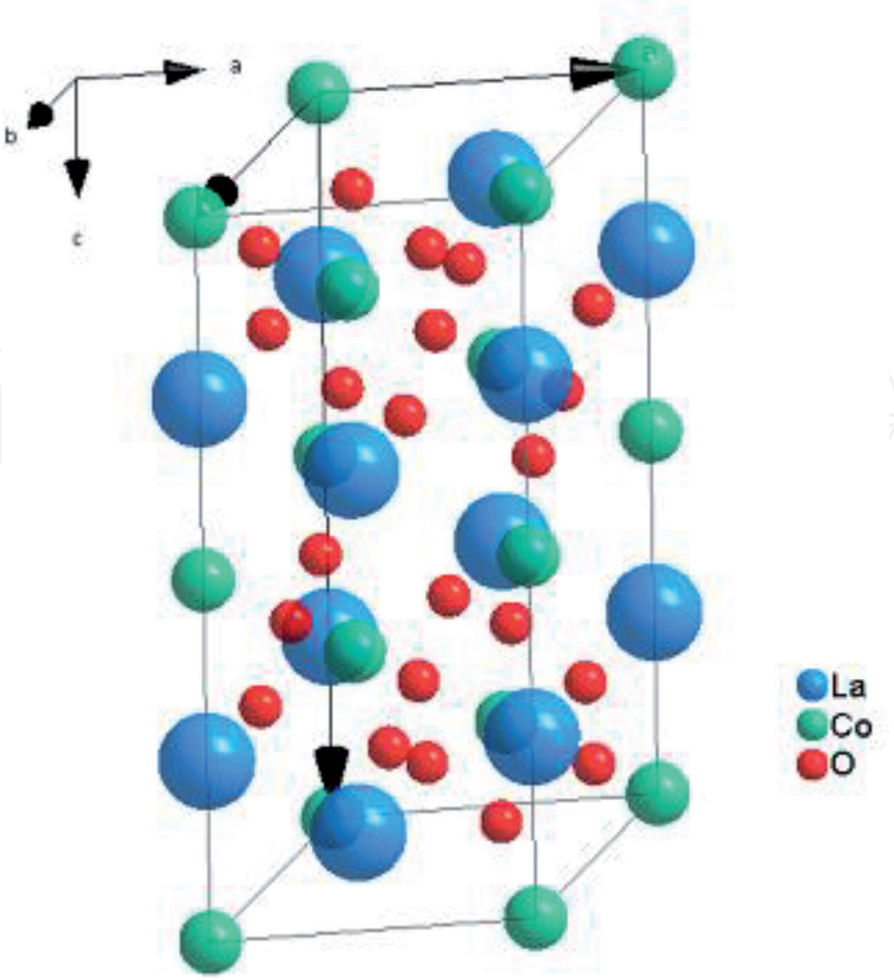


Figure 1.
The crystal structure of rhombohedral $LaCoO_3$.

Despite these various methods, some technological applications are still limited for $LaCoO_3$ compounds. Therefore, knowledge of the preparation conditions and optimization of the technical parameters are key challenges.

The advantages like low temperatures used during processing of wet preparation routes lead to oxide perovskite powders with high-purity nanoparticles. However, these techniques cannot achieve full industrial potential. For instance, major drawbacks of these methods are the high costs of raw materials, the large quantity of gaseous by-products and waste products such as nitrates, acetates, and additional chelating agents used as precursors. The use of such materials requires elaborate systems for gas collection and storage since the by-products are poisonous. Their significant toxicity is not environmentally friendly, making it not sustainable for large-scale applications. In addition to that, these methods involve many stages during the synthesis process. One way to circumvent that is to seek solutions for adapting clean processing routes to specific needs of the products without altering the physical and chemical properties of the resulting powders. For instance, if particle-size distribution is not especially required for certain applications, solid-state synthesis route has superior advantage over wet processing routes owing to its simplicity, less equipment requirements, and ease of scaling up for industrial production.

The elimination of wet processing for perovskite powder preparation means that products will cost less both ways, to produce as well to buy, and have an important economic advantage. In addition, by mixing dry powdered precursors in the

stoichiometric ratios followed by heating to obtain the desired reaction product, at the end of the reaction, there is no waste to dispose. In this way, the method is also environmentally friendly.

The overall price of oxide perovskite powders is strongly influenced by the industrial production route. Solid state reaction technology is resource- and energy-saving. The processing route allows one to obtain the reaction products readily in one step by using less expensive precursors, without waste products. The upscale of solid-state synthesis route resumes to batch production. This is different from flow processing which is a continuous production technique that has inflexibility to adjust if the case. Additionally, the absence of waste and by-products is another major positive aspect regarding the environmental impact of the entire production process. This is why we consider this method useful for both environmental protection and industrial use.

In solid state reaction, rates are typically diffusion-limited; consequently, decreasing the diffusion distances through intimate mixing of reactants possibly contributes to overcome the diffusion barrier in addition to high temperature during the thermal treatment. The characteristics of the starting materials impact the area of contact between the reacting particles with influence of the rate of reaction.

During the heating regime, a non-isothermal transformation takes place, and during the dwell regime, an isothermal transformation takes place. A significant kinetic parameter for studying the phase transformation of precursors is the activation energy E_a, representing the energy barrier for atoms and molecules to move and rearrange. For a given differential scanning calorimetry curve with the heating rate β, one observes the maximum reaction rate at the peak temperature T.

In this study, the kinetic parameters of solid state transformations are determined from the maximum reaction rate at the peak temperature T. For a set of differential scanning calorimetry curves under a constant heating rate, the kinetic transformation is described with the mathematical expression of Kissinger Eq. 2 [27]:

$$\frac{d\left(\frac{\ln\beta}{T^2}\right)}{d\left(\frac{1}{T}\right)} = -\frac{E}{R} \tag{2}$$

where β is the heating rate, E_a is the activation energy, T is the absolute temperature corresponding to maximum process rate, and R is the gas constant.

For the processing the choice of dwell temperature was taking in account Tammann's temperature described as the temperature above which its constitutive cations become mobile so that their bulk diffusion is possible [28, 29].

The electrical conduction phenomenon in perovskite materials is very important since many properties depend on it. There is a strong correlation between the electrical conductivity of the materials, temperature, and the nature of the sample analyzed.

In bulk materials, two types of conductivity phenomena occur: long-range conductivity and localized transport oxygen vacancies. The conduction mechanism can be ionic, electronic, or both. The proportion of ionic to electronic conduction in the materials varies upon temperature and the purity of material. The variation of electrical conductivity with temperature is explained by Eq. (3):

$$\sigma = A\exp^{\frac{-E_a}{KT}} + B\exp^{\frac{-E_{ab}}{KT}} \tag{3}$$

Eq. (4) describes the phenomena at higher temperatures where the intrinsic conduction process dominates.

$$\sigma = A\exp^{\frac{-E_a}{KT}} \tag{4}$$

For both equations, E_a and E_b are the activation energy for the intrinsic and extrinsic conduction processes, respectively, A and B are constants, T is the absolute temperature, and K is the Boltzmann constant.

2. Experiment

2.1 Material preparations

The formation of the perovskite phase via solid state reaction was done under controlled rates for heating and cooling as well as for the dwell of thermal treatment. A 2°C/min rate of heating and cooling was selected. Preparatory trials were carried out in order to find the suitable temperature for dwell covering 600–1000°C.

Equimolar quantities of La_2O_3 and Co_3O_4 powders from Aldrich, with >99.8% purity, were mixed and ground thoroughly in agate mortar. The mixing was done with isopropanol from Chimopar SA, purity >96%. For the thermal treatment, the powder in alumina crucibles was placed in chamber furnace. Once the powder was synthesized, compacted ceramics were prepared by uniaxial pressing technique. After this, they were submitted for sintering. Similarly, preparatory trials were performed to find out the proper sintering thermal treatment.

2.2 Materials characterization

The crystalline structures of the prepared powders were characterized by heating in chamber furnace, environmental air atmosphere, at 50°C increments, making X-ray diffraction measurements. A MiniFlex 600 Rigaku analyzer was used. 2θ scans were recorded between 5 and 90° and a speed of 1°/min, with resolution of 0.1°/step. The as-obtained reflexion patterns are indexed by using the Inorganic Crystal Structure Database (ICSD). Lattice constants and quantitative values for the identified phases are obtained from the fit to the corresponding X-ray diffraction spectra by using the PDXL powder diffraction analysis package from Rigaku. The microstructure and morphology of the as-prepared powders were examined using a scanning electron microscope VP CARL ZEISS (Field Emission Scanning Electron Microscope—FESEM) with LaB_6 cathode enabling 2-nm resolution. Specimens of powders were prepared by depositing it on a conductive carbon-based double-faced adhesive tape. Differential scanning calorimetry (DSC) and thermogravimetric analysis (TGA) measurements were carried out on precursors and their equimolar mixture using STA 449 F5 Jupiter® from NETZSCH-Gerätebau GmbH. The instrument is equipped with Proteus® software to carry out the measurement and evaluation of the resulting data. The DSC/TG curves are recorded up to 1273 K, with a heating rate of 10 K/min.

The analyses of electrical properties of the sample were carried out from 133 to 513 K using Alpha-A Novocontrol Technologies Novocontrol GmbH analyzer in conjunction with a continuous nitrogen flow cryostat.

3. Results

3.1 Thermal behavior

Thermal analysis results of precursors, **Figure 2**, indicate that Co_3O_4 powder, in red color, is stable below 1023 K while La_2O_3 powder, in black color, exhibits several steps of mass loss during the heating regime. La_2O_3 precursor features three weight-loss regions. The first, a gradual weight loss not shown here, is related to

the dehydration of free and physically absorbed molecular water and structural water from the precursor powder. The second and third regions, more pronounced, are associated with the dehydration process from $La(OH)_3$ to La_2O_3 via $LaOOH^-$, according to the chemical reactions described by Eqs. (5) and (6), respectively:

$$La(OH)_3 \rightarrow LaOOH^- + H_2O \quad (5)$$

$$2LaOOH^- \rightarrow La_2O_3 + H_2O \quad (6)$$

The total percent weight loss is around 1.88%. The first step, not shown here, of weight loss was 0.04%. The next steps correspond to the decomposition of $La(OH)_3$. The weight loss in following step was around 0.87%, and in the third step was 0.98%. However, it is well known that $La(OH)_3$ can react relatively fast with the water of the atmosphere to form hydroxyl phase [28]. The corresponding endothermic peaks on the differential scanning calorimetry curve appeared at 581 K and 910 K respectively. The corresponding areas are −23.44 and −15.34 μVs/mg, respectively.

The mixture of Co_3O_4 and La_2O_3 powder precursor, as can be seen in **Figure 3**, has a weight-loss step, associated with the presence of the La_2O_3, and after 1023 K, an endothermic event is detected around 1073 K. Previous studies have found similar features [30]. This is attributed to the ongoing dehydration of LaO(OH) and formation of $LaCoO_3$ from a solid state reaction of lanthanum and cobalt oxides, following Eq. (7):

$$La_2O_3 + Co_3O_4 \rightarrow LaCoO_3 \quad (7)$$

No significant thermic effect was registered at higher temperatures. The corresponding endothermic peaks on the differential scanning calorimetry curve appeared at 1073 K and the area of −147.7, −36.58, and −48.09 μVs/mg, respectively.

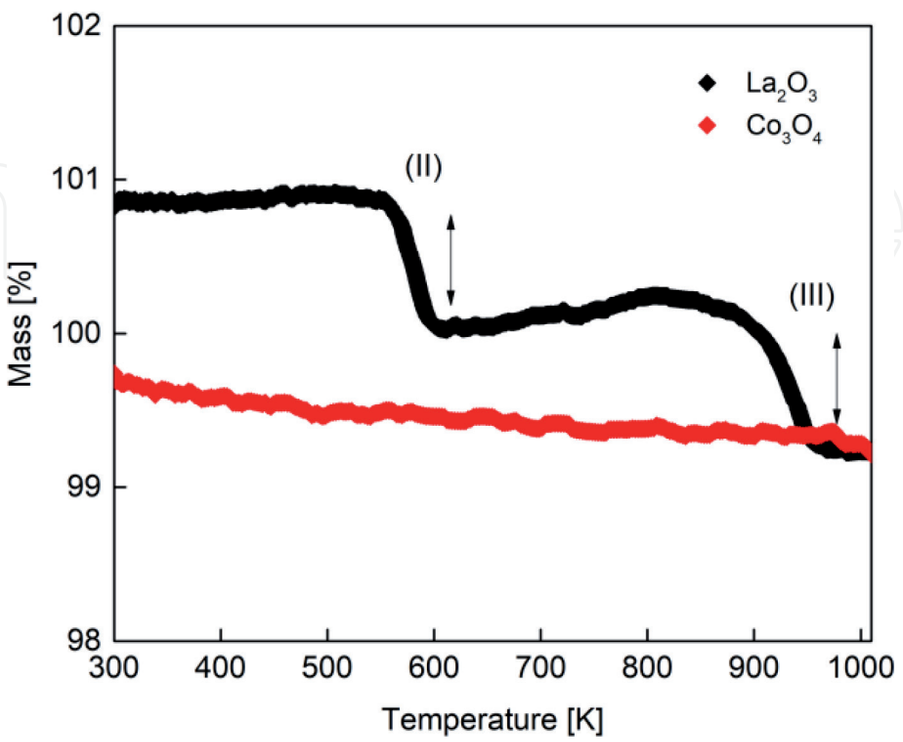


Figure 2.
Weight-loss % diagram for Co_3O_4 powder, in red color, and La_2O_3 powder, in black color.

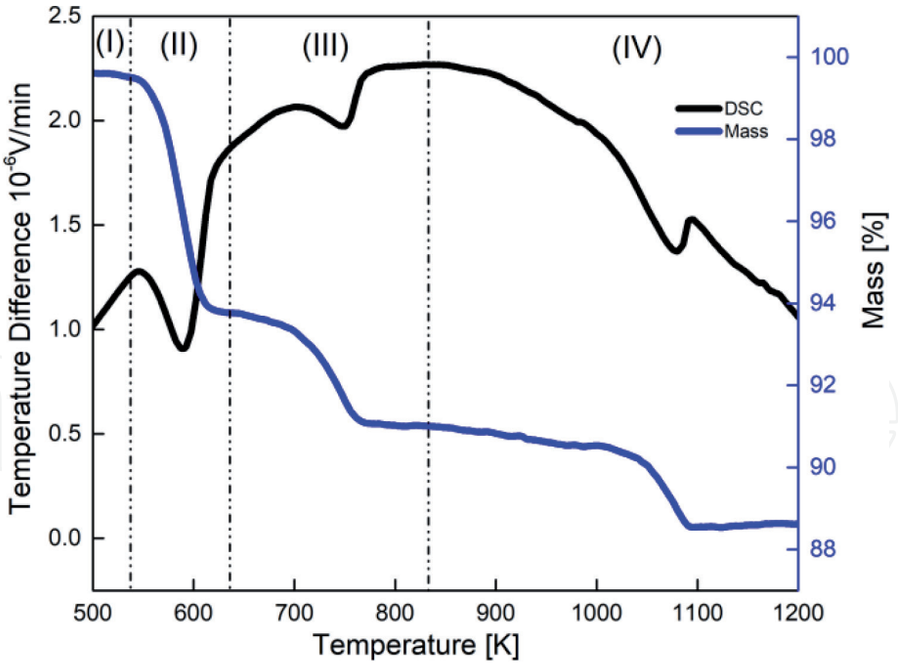


Figure 3.
DSC-TGA plot of Co_3O_4 and La_2O_3 precursor powders in mixture.

The kinetic analysis of phase change for a series of non-isothermal tests, **Figure 4**, is applied to estimate the activation energy. This analysis was performed for third observed exothermal reaction from differential scanning calorimetry data of phase transformation process. The peak temperature T depends on the evolution of the sample with the heating rate. The dynamic heating rate influences the observed peak temperature T of thermal events. These correspond to the variations of growth and phase change rate with temperature. The new phase formation rate depends on temperature and is independent of time. It is observed, in this reaction, the peak temperature has the tendency to slightly shift to the higher temperatures as the heating rates increase.

For polycrystalline reactants, the kinetic process depends on factors like particle size and shapes of the reacting particles, overlapping effects during the formations of the new phase, etc. Solid state reactions are complex and the evaluation of kinetic parameters is helpful for the development of approaching the preparation. In this evaluation, we made the assumption of first order of reaction. From the plot of rate of reaction $\ln(\beta/T^2)$ versus the reciprocal of absolute temperature, **Figure 5**, of as-mixed Co_3O_4 and La_2O_3 powder precursors, an E_a = 223 kJ/mol is obtained, which seems to be in good agreement with earlier results reported [31].

3.2 X-ray diffraction investigation

The analysis of X-ray diffraction pattern corresponding to unmixed and mixed precursors as function of temperature treatment is shown in **Figure 6**. In the lowest position of the diagram, the unmixed La_2O_3 and Co_3O_4 powder precursors are displayed. Going up in the diagram, the mixture of La_2O_3 and Co_3O_4 powder precursors at room temperature is indicated. The La_2O_3 powder precursor is tetragonal La_2O_3 (space group P-3m1) with a = b = 3.933 Å and c = 6.132 Å [32]. Traces of hexagonal $La(OH)_3$ (space group P63/m) are detected. The corresponding lattice constant values are a = b = 6.529 Å and c = 3.859 Å. Co_3O_4 powder indicates that the precursor is single-phase, with cubic crystal symmetry (space group Fd-3m) [32]. The lattice constant value obtained from fit to data is a = 8.038 Å.

Upon thermal treatment, which is done to favor the formation of end products of perovskite of $LaCoO_3$, the X-ray diffraction patterns show the formation of the perovskite phase. The XRD data confirm the perovskite $LaCoO_3$ phase is converted upon heat treatment starting at 1023 K, growing progressively with increasing temperature up to 1273 K. This is followed by a gradual smoothing of the peak intensities of the precursor phases. The resulting powder can be indexed on the basis of a rhombohedral unit cell; the peaks around $2\theta = 33.12°$ are bifurcated,

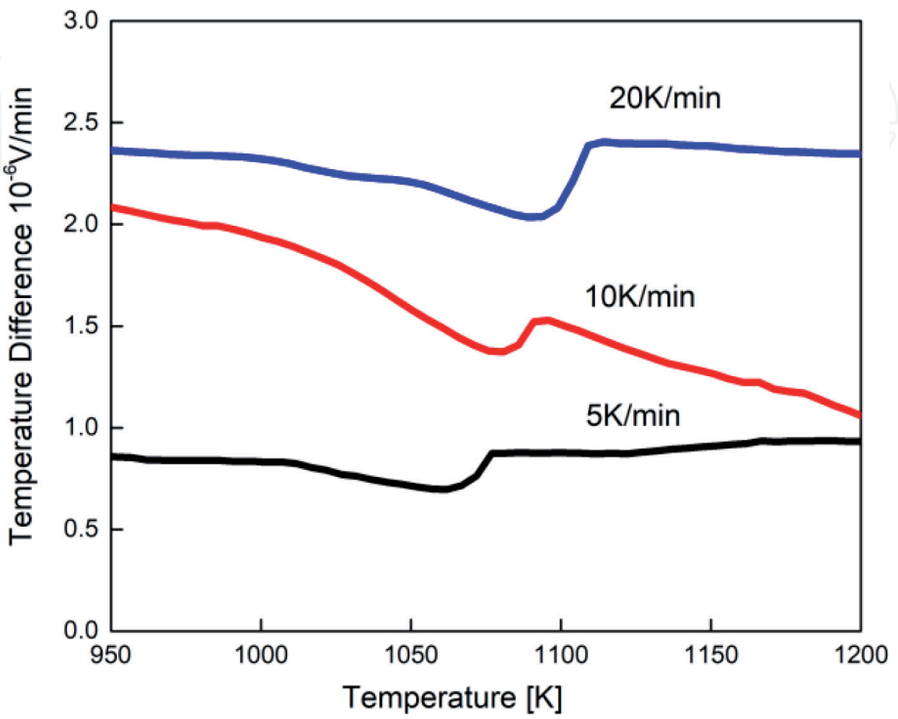


Figure 4.
Differential scanning calorimetry curves of as-mixed Co_3O_4 and La_2O_3 powder precursors at different heating schedules.

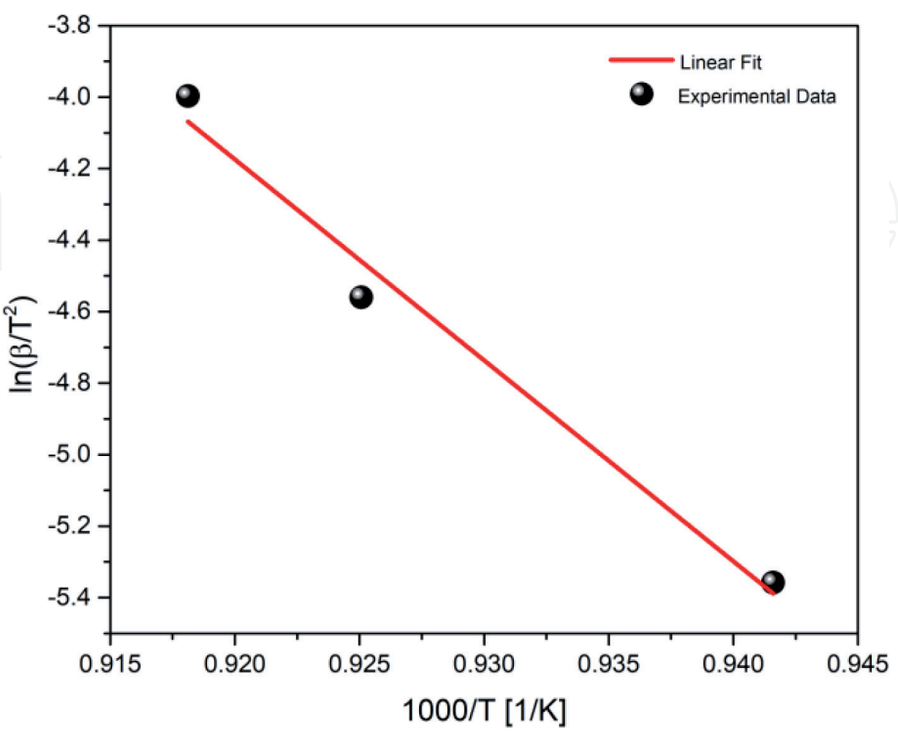


Figure 5.
Variation of $\ln(\beta/T^2)$ plot for a set of differential scanning calorimetry scans with different heating rates.

which is the characteristic peak for the rhombohedral structure and confirmed by the experimental X-ray results as well as previous studies [33, 34].

The prepared $LaCoO_3$ has trigonal crystal symmetry space group R-c3 [35, 36]. The lattice constant values obtained from fit to data are a = b = 5.444 Å and c = 13.104 Å.

The average particle size is calculated from the XRD pattern using Debye and Scherrer formula, Eq. (8):

$$d = \frac{K\lambda}{\beta \cos\theta} \tag{8}$$

where K = 0.94 is the Scherrer constant, λ is the wavelength of the X-ray source used, β is the full width at the half maxima, and θ is the Bragg diffraction angle.

The result obtained for the average crystallite size by Scherrer's equation is 294 Å.

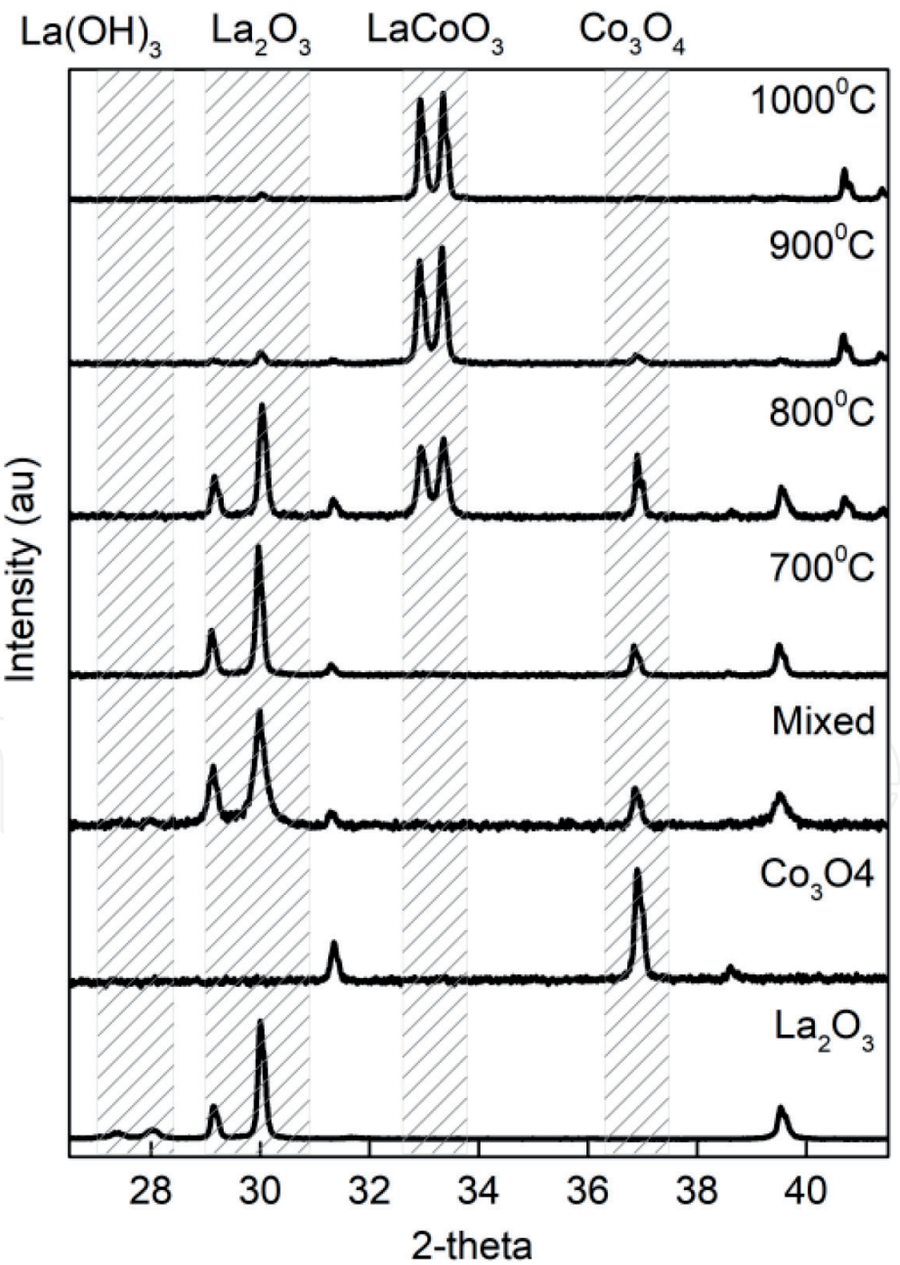


Figure 6.
Room temperature X-ray diffraction patterns of un/mixed La_2O_3 and Co_3O_4 powder precursors and $LaCoO_3$ powders according to the thermal treatment.

3.3 Microscopy analysis

Scanning electron micrograph of $LaCoO_3$ powders obtained by solid state synthesis at 1273 K is displayed in **Figure 7**. The perovskite $LaCoO_3$ powders obtained consist of pre-sintered conglomerates of grains. The agglomeration tendency is due to the high calcination temperature employed to obtain the single phase. The reaction product has well-defined shape and less uniform grain size distribution. The high-temperature calcination results in severe agglomeration. The sintering of many crystallites during high thermal treatment resulted in the larger grains, which are polycrystals. The grain limits and triple junction points are well defined.

3.4 Electric properties

In **Figure 8**, we show the electrical conductivity of our polycrystalline pellets pressed and sintered at 1173 K. Greater conductivity differences are noticed to depend on the temperature. The tendency of $LaCoO_3$ electrical conductivity is to increase when temperature is rising. This behavior of electrical conductivity in relation to the temperature indicates the process is thermally activated, which is characteristic for semiconductors. For our $LaCoO_3$ sample, semiconducting behavior appears at temperatures above 353 K, whereas metallic behavior was observed at temperatures below 353 K. This is in accordance with the previous statements that $LaCoO_3$ is ionic at elevated temperatures. The electrical conductivity is p-type for both ambient and elevated temperatures. With semiconductors, there are insufficient mobile carriers at low temperatures and resistance is high; but, as we heat the material, more and more of the lightly bound carriers escape and become free to conduct. Electrons are excited over the band gap and occupy energy levels in conductivity band whereas holes are created in valence band. The band gap in the metal is small and the electrons can easily jump to conduction band. For the metallic behavior with increasing temperature above absolute zero, the flowing electrons

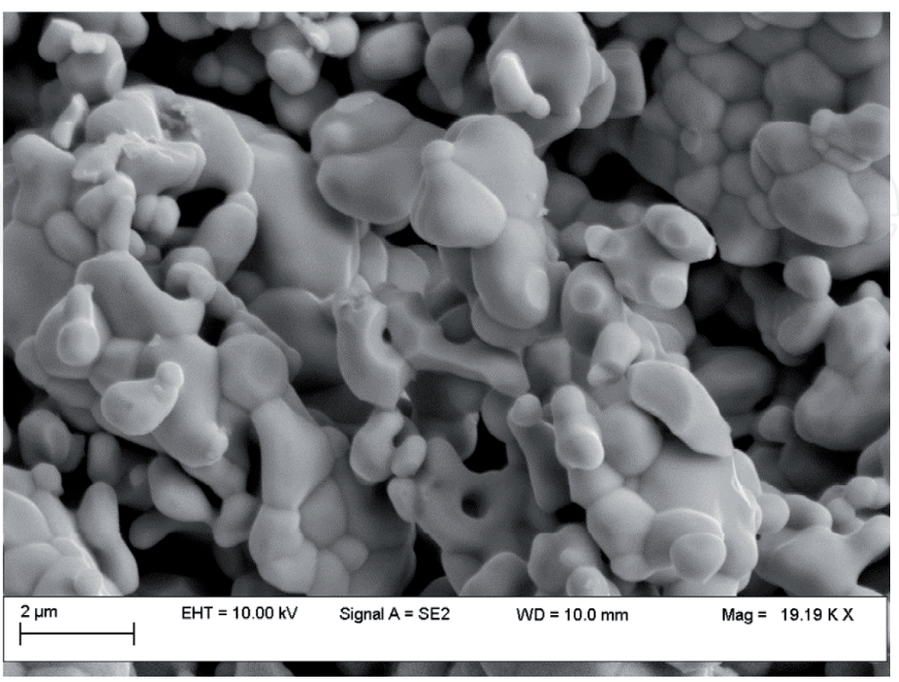
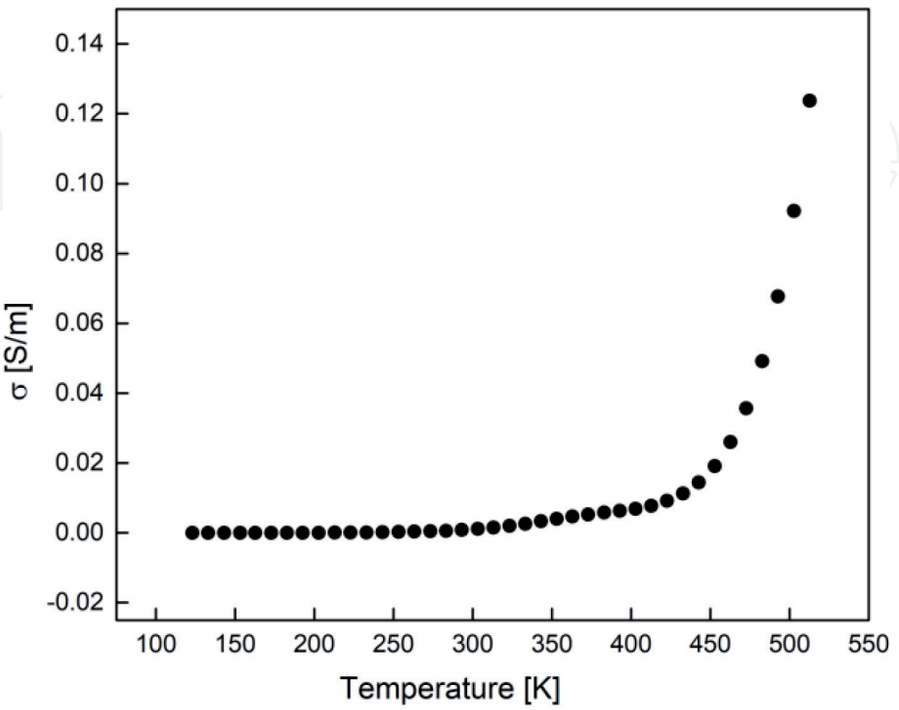
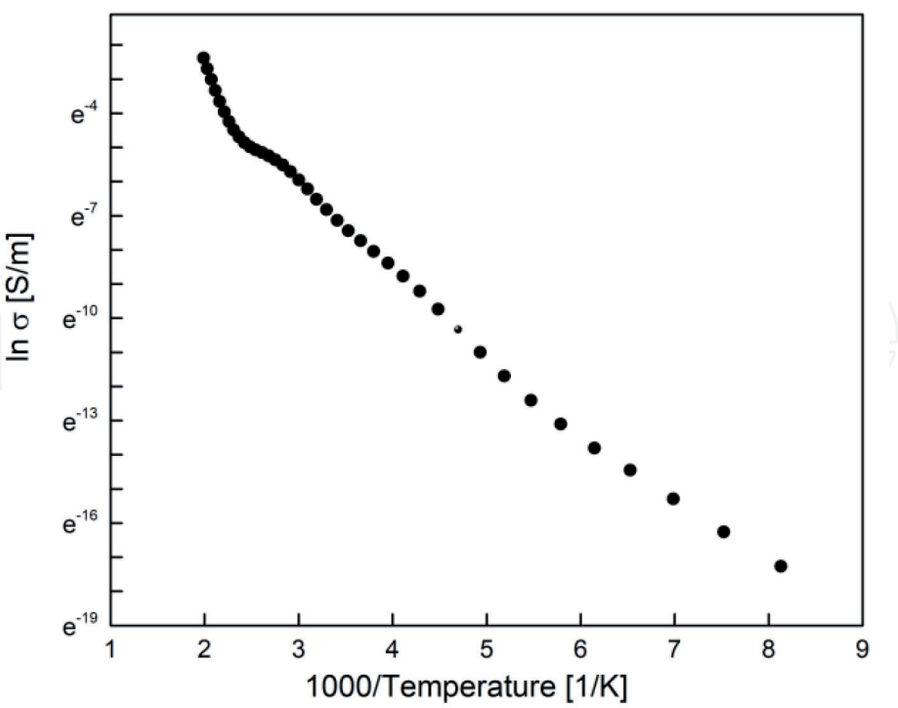


Figure 7.
SEM micrograph of $LaCoO_3$ powder.

will run into the atoms in the lattice. This will cause the atoms to move slightly out of their lattice sites and to interfere with electrons that travel freely. Effectively, they start to block electrons on their path, causing electrons to scatter. The change in slope of the conductivity-temperature plot is assumed to be the onset of ionic conductivity. $LaCoO_3$ is a mixed conductor with contributions from ionic conductivity and electronic conductivity.



a)



b)

Figure 8.
$LaCoO_3$ total conductivity σ depending on absolute temperature in (a) and lnσ depending on absolute temperature in (b).

Variation of the electrical conductivity with temperature obeys Arrhenius formula, Eq. (9), and is calculated based on the following:

$$\sigma = \sigma_0 \exp\left(\frac{-E_a}{KT}\right) \tag{9}$$

where σ_0 is the pre-exponential factor, E_a is the activation energy, K is the Boltzmann constant, and T is the absolute temperature. The activation energy of the electrical conductivity was found to be E_a = 74 kJ/mol.

For the undoped $LaCoO_3$ oxide, the oxygen non-stoichiometry is considered to determine the carriers for the conduction phenomena. This is believed to be caused by the oxygen elimination with increase in the temperature (**Figure 9**).

The Kröger-Vink set of conventions are used to describe electric charge and lattice position for point defect species in crystals. The following ions and vacancies are used: La^{3+}, Co^{2+}, Co^{3+}, Co^{4+}, O^{2-}, oxygen vacancies. Making use of these in Eq. (10), the defect equilibrium between the charge species and oxygen partial pressure can explain the increase of partial pressure of oxygens:

$$2\,Co_{Co}^{\bullet} + O_O^x = V_O^{\bullet\bullet} + 2\,Co_{Co}^x + \frac{1}{2}O_2\,(g) \tag{10}$$

where $Co_{Co}^x = Co^{3+}$, $Co_{Co}^{\bullet} = Co^{4+}$ and $O_O^x = O^{2-}$.

Eq. (11) expresses the charge disproportion defect as follows:

$$2\,Co^{3+} \leftrightarrow Co^{2+} + Co^{4+} \tag{11}$$

When a voltage is applied to our sintered $LaCoO_3$ sample, a current flow is observed. At a given temperature, the type of charge carrier species is not defined. Because of this, it is useful to depict the conductivity dependence on temperature. The existence of ions is assured by definition, mixed conductors being ionic

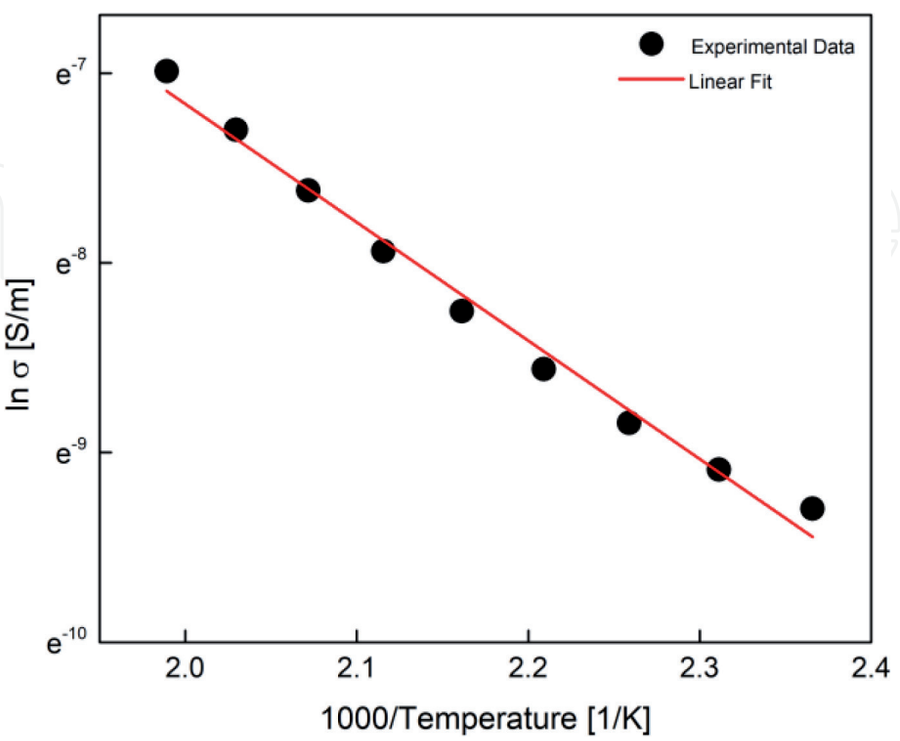


Figure 9.
Variation of dc conductivity (σ) with inverse of absolute temperature for $LaCoO_3$.

compounds. Ionic defects have their most pronounced effect on transport properties, which are ionic conductivity and diffusion. For $LaCoO_3$ samples, the oxygen vacancies are the mobile ionic defects.

4. Conclusions

In this study, we successfully used solid state synthesis as a dry method for preparation of rhombohedral lanthanum cobaltite $LaCoO_3$ perovskite-type oxides.

The solid state synthesis process is thermally activated and requires high temperatures. The X-ray diffraction analysis suggests that $LaCoO_3$ phase nucleates readily at 973 K. The formation of $LaCoO_3$ occurs gradually with increasing temperature, at the expense of precursors' consumption. At 1273 K, the reaction is essentially complete. Thermal analysis suggests that the reaction is accompanied by reversible transformation of $La(OH)_3$ into La_2O_3, which is a native surface phase of the oxide phase. The reaction kinetics is strongly mediated by Co_3O_4 transformation. Co_3O_4 starts to transform before its decomposition temperature. The overall electronic transport properties exhibited by the prepared powders are typically ionic at elevated temperatures (above 353 K) and are mediated by presence of oxygen vacancy.

The interrelationship between structure and properties is a key element of materials science and engineering. Thinking of the variety of oxide perovskite materials, each particular application is based on a certain functional property of the material. Most macroscopic properties observed in bulk (e.g., crystalline quality, ionic conductivity, density, etc.) are the consequence of the constituent particles' properties of the material. For applications, it is essential to know the relation between material microstructure and the macroscopic properties in order to adjust its performance to more specific requirements and also to keep the fabrication costs low. Properties like ionic conductivity, for example, make the perovskite material promising to be used as a solid electrolyte for solid oxide fuel cells (SOFC). Similarly, ferroelectric and piezoelectric behaviors lead to potential applications for thermistor, actuator, and piezoelectric transducers, and the property of superconductivity to superconductors.

We consider this method to be beneficial for both environmental protection and industrial applications because it does not have by-products or waste at the end of the reaction and the precursors are not expensive. In addition to this, an important advantage of this method is the sustainability to scale up the process. We recommend this for batch production which allows flexibility to adjust the process as required for a specific application. There is no need for additional facilities to collect the gaseous by-products or the waste to collect it and dispose it.

With appropriate optimization, this method we applied to $LaCoO_3$ can be applied to other perovskites; the synthesizing parameters like reaction time and temperature should be obtained by exploration as performed with the recipe presented in this chapter.

We conclude the present work stating that using this conventional method as solid state reaction allows obtaining highly single-phase $LaCoO_3$ powders for applications and uses of advanced functional materials.

Acknowledgements

This work was supported by the National Authority for Scientific Research and Innovation/Romanian Ministry of Education and Research, project "RESTORE"—117/16.09.2016 ID/Cod My SMIS: P_37_595/104958.

Conflict of interest

The authors state that there is no conflict of interest associated with this work.

Thanks

The authors would like to thank Dr. Amalia Soare for taking the SEM photograph.

Author details

Mirela Dragan[1*], Stanica Enache[1], Mihai Varlam[1] and Konstantin Petrov[1,2]

1 National R&D Institute for Cryogenic and Isotope Technologies, Ramnicu Valcea, Romania

2 Academician Evgeni Budevski Institute of Electrochemistry and Energy Systems, Sofia, Bulgaria

*Address all correspondence to: mirela.dragan@icsi.ro

IntechOpen

© 2019 The Author(s). Licensee IntechOpen. This chapter is distributed under the terms of the Creative Commons Attribution License (http://creativecommons.org/licenses/by/3.0), which permits unrestricted use, distribution, and reproduction in any medium, provided the original work is properly cited. CC BY

References

[1] Lin Q, Yang X, Lin J, Guo Z, He Y. The structure and magnetic properties of magnesium-substituted $LaFeO_3$ perovskite negative electrode material by citrate sol-gel. International Journal of Hydrogen Energy. 2018;**43**(28):12720-12729. DOI: 10.1016/j.ijhydene.2018.03.156

[2] Goswami S, Bhattacharya D. Magnetic transition at ~150 K in nanoscale $BiFeO_3$. Journal of Alloys and Compounds. 2018;**738**:277-282. DOI: 10.1016/j.jallcom.2017.12.107

[3] Presto S, Kumar P, Varma S, Viviani M, Singh P. Electrical conductivity of NiMo-based double perovskites under SOFC anodic conditions. International Journal of Hydrogen Energy. 2018;**43**(9):4528-4533. DOI: 10.1016/j.ijhydene.2018.01.066

[4] Zhang F, Zhang X, Jiang G, Li N, Hao Z, Qu S. H_2S selective catalytic oxidation over Ce substituted $La_{1-x}Ce_xFeO_3$ perovskite oxides catalyst. Chemical Engineering Journal. 2018;**348**:831. DOI: 10.1016/j.cej.2018.05.050.p

[5] Wang WL, Meng Q, Xue Y, Weng X, Sun P, Wu Z. Lanthanide perovskite catalysts for oxidation of chloroaromatics: Secondary pollution and modifications. Journal of Catalysis. 2018;**366**:213-222. DOI: 10.1016/j.jcat.2018.07.022

[6] Fang M, Yao X, Li W, Li Y, Shui M, Shu J. The investigation of lithium doping perovskite oxide $LiMnO_3$ as possible LIB anode material. Ceramics International. 2018;**44**(7):8223-8231. DOI: 10.1016/j.ceramint.2018.02.002

[7] Yao C, Zhang H, Liu X, Meng J, Zhang X, Meng F, et al. Characterization of layered double perovskite $LaBa_{0.5}Sr_{0.25}Ca_{0.25}Co_2O_{5+\delta}$ as cathode material for intermediate-temperature solid oxide fuel cells. Journal of Solid State Chemistry. 2018;**265**:72-78. DOI: 10.1016/j.jssc.2018.05.028

[8] Heikes R, Miller RC, Mazelsky R. Magnetic and electrical anomalies in $LaCoO_3$. Physica. 1964;**30**(8):1600-1608. DOI: 10.1016/0031-8914(64)90182-X

[9] Menyuk N, Dwigh K, Raccah PM. Low temperature crystallographic and magnetic study of $LaCoO_3$. Journal of Physics and Chemistry of Solids. 1964;**28**(4):549-556. DOI: 10.1016/0022-3697(67)90085-6

[10] Enache S, Dragan M, Soare A, Ebrasu DI, Zaulet A, Varlam M, et al. One step solid-state synthesis of lanthanum cobalt oxide perovskites as catalysts for oxygen evolution in alkaline media. Special Issue of Bulgarian Chemical Communications, Sofia, Bulgaria. 2018;**50**(A):127-132

[11] Ebrasu DI, Zaulet A, Enache S, Dragan M, Carcadea E, Varlam M, et al. Electrochemical characterization of metal oxide as catalysts oxygen evolution in alkaline media. Special Issue of Bulgarian Chemical Communications, Sofia, Bulgaria. 2018;**50**(A):133-138

[12] Cullity BD, Graham CD. Introduction to Magnetic Materials. 2nd ed. Hoboken, New Jersey, United States: Wiley-IEEE Press; 2008. 171p. DOI: 10.1002/9780470386323

[13] Greenwood NN, Earnshaw A, editors. Chemistry of the Elements. 2nd ed. Oxford, United Kingdom: Butterworth-Heinemann; 1997. 1113p. DOI: 10.1016/B978-0-7506-3365-9.50032-8

[14] Zhu H, Zhang P, Dai S. Recent advances of lanthanum-based perovskite oxides for catalysis. ACS

Catalysis. 2015;**5**(11):6370-6385. DOI: 10.1021/acscatal.5b01667

[15] Chainani A, Mathew M, Sarma DD. Electron-spectroscopy study of the semiconductor-metal transition in $La_{1-x}Sr_xCoO_3$. Physical Review B. 1992;**46**(16):9976-9983. DOI: 10.1103/PhysRevB.46.9976

[16] Ma CL, Cang J. First principles investigation on the band gap of the ground state of $LaCoO_3$. Solid State Communications. 2010;**150**(41-42): 1983-1986. DOI: 10.1016/j.ssc.2010.08.023

[17] Shannon RD. Revised effective ionic radii and systematic studies of interatomic distances in halides and chalcogenides. Acta Crystallographica, Section A: Crystal Physics, Diffraction, Theoretical and General Crystallography. 1976;**32**(5):751-767. DOI: 10.1107/S0567739476001551

[18] Radaelli PG, Cheong SW. Structural phenomena associated with the spin-state transition in $LaCoO_3$. Physical Review B. 2002;**66**(9):094408-094417. DOI: 10.1103/PhysRevB.66.094408

[19] Kobayashi Y, Mitsunaga T, Fujinawa G, Arii T, Suetake M, Asai K, et al. Structural phase transition from rhombohedral to cubic in $LaCoO_3$. Journal of the Physical Society of Japan. 2000;**69**(1):3468-3469. DOI: 10.1143/JPSJ.69.3468

[20] Mizusaki J, Mima Y, Yamauchi S, Fueki K, Tagawa H. Nonstoichiometry of the perovskite-type oxides $La_{1-x}Sr_xCoO_{3-\delta}$. Journal of Solid State Chemistry. 1989;**80**(1):102-111. DOI: 10.1016/0022-4596(89)90036-4

[21] Xu R, Su Q. High-temperature synthesis. In: Xu R, Pang W, Huo Q, editors. Modern Inorganic Synthetic Chemistry. Amsterdam, Netherlands: Elsevier; 2011. pp. 9-38. DOI: 10.1016/B978-0-444-53599-3.10002-2

[22] Rojac T, Kosec M. Mechanochemical synthesis of complex ceramic oxides. In: Sopicka-Lizer M, editor. High-Energy Ball Milling. Sawston, Cambridge, United Kingdom: Woodhead Publishing; 2010. pp. 113-148. DOI: 10.1533/9781845699444.2.113

[23] Huízar-Félix AM, Hernández T, de la Parra S, Ibarra J, Kharisov B. Sol–gel based Pechini method synthesis and characterization of $Sm_{1-x}Ca_xFeO_3$ perovskite $0.1 \leq x \leq 0.5$. Powder Technology. 2012;**229**:290-293. DOI: 10.1016/j.powtec.2012.06.057

[24] Manukyan KV. Solution combustion synthesis of catalysts. In: Borovinskaya IP, Gromov AA, Levashov EA, Maksimov YM, Mukasyan AS, Rogachev AS, editors. Concise Encyclopedia of Self-Propagating High-Temperature Synthesis. Amsterdam, Netherlands: Elsevier; 2017. pp. 347-348. DOI: 10.1016/B978-0-12-804173-4.00137-X

[25] Sakka S. Sol–gel process and applications. In: Somiya S, editor. Handbook of Advanced Ceramics. 2nd ed. Cambridge, Massachusetts, United States: Academic Press; 2013. pp. 883-910. DOI: 10.1016/B978-0-12-385469-8.00048-4

[26] Agrawa D. Microwave sintering of ceramics, composites and metal powders. In: Fang ZZ, editor. Sintering of Advanced Materials. Sawston, Cambridge, United Kingdom: Woodhead Publishing Series in Metals and Surface Engineering; 2010. pp. 222-248. DOI: 10.1533/9781845699949.2.222

[27] Kissinger HE. Reaction kinetics in differential thermal analysis. Analytical Chemistry. 1957;**29**(11):1702-1706. DOI: 10.1021/ac60131a045

[28] Tammann G, Mansuri QA. Metallographische Mitteilungen aus dem Institut für physikalische Chemie der Universität Göttingen CXIII. Zur

Rekristallisation von Metallen und Salzeneitschrift für anorganische und allgemeine Chemie. 1923;**126**(1):119-128. DOI: 10.1002/zaac.19231260109

[29] Tammann G. Zur Molekular-Dynamik in Kristallen. Nachrichten von der Gesellschaft der Wissenschaften zu Göttingen, Mathematisch-Physikalische Klasse. Göttingen, Germany: Deutsche Forschungsgemeinschaft e.V; Vol. 281930. pp. 227-254. Available http://www.digizeitschriften.de/dms/resolvepn/?PID=GDZPPN002508184

[30] Jiawen D, Yanli W, Weili S, Youngxiu L. Preparation of $La(OH)_3$ and La_2O_3 with rod morphology by simple hydration of La_2O_3. Journal of Rare Earths. 2006;**24**(4):440-442. DOI: 10.1016/S1002-0721(06):60139-7

[31] Walter D. Kinetic analysis of the transformation from lanthanum hydroxide to lanthanum oxide. Zeitschrift für Anorganische Chemie. 2006;**632**(12-13):2165-2165. DOI: 10.1002/zaac.200670177

[32] Aldebert P, Traverse JP. Etude par diffraction neutronique des structures de haute temperature de La_2O_3 et Nd_2O_3. Materials Research Bulletin. 1979;**14**(3):303-323. DOI: 10.1016/0025-5408(79)90095-3

[33] Liu X, Prewitt CT. High-temperature X-ray diffraction study of Co_3O_4: Transition from normal to disordered spinel. Physics and Chemistry of Minerals. 1990;**17**(2): 168-172. DOI: 10.1007/BF00199669

[34] Ozawa M, Onoe R, Kato H. Formation and decomposition of some rare earth (RE = La, Ce, Pr) hydroxides and oxides by homogeneous precipitation. Journal of Alloys and Compounds. 2006;**408-412**:556-559. DOI: 10.1016/j.jallcom.2004.12.073

[35] Dragan M, Misture S. In-situ analysis of chemical expansion and stability of SOFC cathodes. Materials Research Society Symposium Proceedings. 2014;**1655**:77-82. DOI: 10.1557/opl.2014.413

[36] Haas O, Struis RPWJ, McBreen JM. Synchrotron X-ray absorption of $LaCoO_3$ perovskite. Journal of Solid State Chemistry. 2004;**177**(3):1000-1010. DOI: 10.1016/j.jssc.2003.10.004